LETTER
PLANETARY SCIENCES

Earth and Planetary Physics
7: 607–614, 2023
doi: 10.26464/epp2023086

Direct evidence for efficient scattering of suprathermal electrons by whistler mode waves in the Martian magnetosphere

Tong Li[1,2], Si Liu[1,2*], Chang Yang[1], FuLiang Xiao[1,2*], HongMing Yang[3], Sai Zhang[1], ZhongLei Gao[1], Qian He[1], QingHua Zhou[1], QiWu Yang[1], and YiHua He[1]

[1]School of Physics and Electronic Sciences, Changsha University of Science and Technology, Changsha 410114, China;

[2]Hunan Provincial Key Laboratory of Flexible Electronic Materials Genome Engineering, Changsha University of Science and Technology, Changsha 410114, China;

[3]School of Electrical and Information Engineering, Changsha University of Science and Technology, Changsha 410114, China

Key Points:

- A unique event is reported in which whistler mode waves are observed exactly corresponding to MAVEN detection of suprathermal electron dropout.
- The diffusion coefficients of the whistler mode waves are calculated by using the measured electric field power.
- These observations suggest that whistler mode waves can cause a decrease in the flux of suprathermal electrons (3–45 eV).

Citation: Li, T., Liu, S., Yang, C., Xiao, F. L., Yang, H. M., Zhang, S., Gao, Z. L., He, Q., Zhou, Q. H., Yang, Q. W., and He, Y. H. (2023). Direct evidence for efficient scattering of suprathermal electrons by whistler mode waves in the Martian magnetosphere. *Earth Planet. Phys.*, *7*(6), 607–614. http://doi.org/10.26464/epp2023086

Abstract: Whistler mode waves are critical emissions in magnetized plasmas that usually influence the electron dynamics in a planetary magnetosphere. In this paper, we present a unique event in the Martian magnetosphere in which enhanced whistler mode waves (~10^{-11} $V^2/m^2/Hz$) with frequency of 0.1 f_{ce}–0.5 f_{ce} occurred, based on MAVEN data, exactly corresponding to a significant decrease of suprathermal electron fluxes. The diffusion coefficients are calculated by using the observed electric field wave spectra. The pitch angle diffusion coefficient can approach 10^{-2} s^{-1}, which is much larger, by ~100 times, than the momentum diffusion coefficient, indicating that pitch angle scattering dominates the whistler–electron resonance process. The current results can successfully explain the dropout of the suprathermal electrons in this event. This study provides direct evidence for whistler-driven electron losses in the Martian magnetosphere.

Keywords: whistler mode waves; diffusion coefficients; electron scattering; Martian magnetosphere

1. Introduction

Whistler mode waves are commonly observed in the magnetosphere of magnetized planets (Shprits et al., 2012), such as Jupiter (Scarf et al., 1979; Shprits et al., 2018; Li W et al., 2021), Saturn (Akalin et al., 2006; Hospodarsky et al., 2008; Kumari and Pandey, 2018), and Earth (Fairfield 1974; Wei XH et al., 2007; Yang QW et al., 2016; Shang XJ et al., 2021; He Q et al., 2022). In particular, whistler mode waves in the terrestrial magnetosphere have been extensively studied due to their critical roles in the acceleration of relativistic electrons (Xiao FL et al., 2014; Gao ZL et al., 2016), penetration of energetic electrons (Li W et al., 2009, 2013; Zhao H and Li X, 2013; Ni BB et al., 2018; Zhao YW et al., 2022), and scattering of relativistic electrons (Liu S et al., 2020; He JB et al., 2021).

First author: T. Li, lt@csust.edu.cn
Correspondence to: S. Liu, liusi@csust.edu.cn
F. L. Xiao, flxiao@126.com
Received 26 AUG 2023; Accepted 06 NOV 2023.
First Published online 08 NOV 2023.

Although there is no intrinsic magnetosphere for Mars, the solar wind squeezes the Martian neutral atmosphere and ionosphere as it rotates (Nagy et al., 2004), leading to a dynamic magnetic field environment at Mars. Several missions, such as the Mars Atmosphere and Volatile EvolutioN (MAVEN) (Jakosky et al., 2015a) and the Tianwen-1 (Wan WX et al., 2020), have been launched, providing an excellent opportunity to investigate the effects of plasma waves on particles in the Martian magnetosphere (Jin TF et al., 2023). Harada et al. (2016) have reported on whistler mode waves with electric and magnetic field wave spectra and suggested that Martian whistler mode waves are generated by anisotropic electrons with energies from 100 eV to 1000 eV. Shane et al. (2019) have shown a ubiquitous energization process of high-energy electrons, and suggested that wave-particle interactions are the most likely candidate to produce such distributions of high-energy electrons. Fowler et al. (2020) have studied wave-particle interactions, and suggested that whistler mode waves can produce efficient pitch angle diffusion of suprathermal electrons. Shane and Liemohn (2021, 2022) have calculated the bounce-averaged diffusion rates of whistler mode waves in a dipole

magnetic field model and again proposed that wave-particle interactions are the most likely candidates to produce pitch angle distributions for suprathermal electrons. However, convincing direct evidence for whistler–particle interactions and their corresponding influence on particle dynamics in the Martian magnetosphere has been lacking.

Here, we present a unique event in which whistler mode waves with frequency of 0.1 f_{ce}–0.5 f_{ce} occurred exactly corresponding to a pronounced decrease of suprathermal electron fluxes in the Martian magnetosphere, based on MAVEN data. To examine whether the whistler mode waves are likely to have been responsible for the observed dropout of the electron fluxes, we calculate the diffusion coefficients by using realistic parameters. Our report is organized as follows: Section 2 describes the correlated observations of waves and electrons; Section 3 presents our calculations of diffusion coefficients of the whistler mode waves; Section 4 discusses the simulation results; Section 5 summarizes the findings of this paper.

2. Observations

MAVEN, the first satellite to explore the evolution of the Martian space environment under the influence of the sun and solar wind, was launched in November 2013 and began collecting data at Mars in November 2014 (Jakosky et al., 2015b). There are eight science instruments on board the MAVEN spacecraft that measure the Martian upper atmospheric and ionospheric properties, including details of the magnetic field, plasma waves, solar wind, solar radiation, and particle fluxes. To analyze this event, we needed data from three instruments carried by MAVEN — the Langmuir Probe and Waves (LPW), the magnetometer (MAG), and the Solar Wind Electron Analyzer (SWEA). The LPW measures the electron density and electric field wave components (Andersson et al., 2015). The MAG obtains ambient magnetic field data and magnetic field wave components (Connerney et al., 2015). The SWEA detects the energy distribution of suprathermal electrons (3–5000 eV) with an energy resolution of 17% ($\Delta E/E$), as well as the angular distributions of these electrons (Mitchell et al., 2016).

Figure 1 shows a brief overview of this event from 05:25:00 UT to 05:26:30 UT on June 20, 2015. The electric field spectra are presented in Figure 1a. The upper and lower white dashed lines represent the f_{ce} and f_{LH}, respectively, where f_{LH} is the lower hybrid frequency. As highlighted by the red dashed line, distinct waves with the peak spectral density ~10^{-11} $V^2/m^2/Hz$ occurred between 05:25:38 UT and 05:26:22 UT on June 20, 2015, which corresponds to the local Martian times between 20.73 LT and 20.81 LT. The wave frequency ~0.1 f_{ce}–0.5 f_{ce} stays between f_{LH} and f_{ce}. Considering that whistler mode is the only solution in the frequency range based on previous theoretical studies (Stix, 1992), the waves mentioned in this event can reasonably be assumed to be whistler waves, even though there is no information about the magnetic field spectrum (Harada et al., 2016). Figure 1b exhibits the observed fluxes of electrons in the energy range 3–100 eV. The suprathermal electrons are mainly composed of photoelectrons from the Martian atmosphere and solar wind/magnetosheath electrons (Xu SS and Liemohn, 2015). The fluxes exhibit a distinct decrease during the period from 05:25:38 to 05:26:05 UT, which coincides exactly with the observation of the whistler mode waves. Specifically, there is a substantial decrease (by a factor of ten) in electron fluxes with energies ~3–45 eV. The pitch angle distribution of the selected energy channels 3 eV, 19 eV, and 43 eV, are shown in Figures 1c–1e, respectively. During the duration of the enhanced whistler mode waves, electron fluxes over all measured energies decrease, especially at small pitch angles. The strong interaction between electrons and whistler mode waves is related to the ambient plasma conditions; this has important effects on electron dynamic variations (Xiao FL et al., 2009a, b). In general, wave-driven scattering loss (acceleration) of electrons is associated with higher (lower) plasma density. Figure 1f plots the background plasma density N_e from LPW data. According to the correlated observation above, the losses of suprathermal electrons are strongly related to the occurrence of whistler mode waves within the relatively dense plasma (~80 cm^{-3}).

To clarify how the magnetic field environment was measured, we present the orbit of the MAVEN spacecraft and the crustal magnetic field at the spacecraft location in Figure 2. The trajectory of the spacecraft in the X_{MSO}–Y_{MSO} and X_{MSO}–Z_{MSO} planes in Mars Solar Orbital (MSO) coordinates is shown in Figures 2a and 2b, respectively. The red star denotes the location of the spacecraft during the occurrence of the enhanced whistler waves. Obviously, the enhanced whistler waves are located on the nightside of Mars's southern hemisphere. Based on the global model of the Martian crustal field (Morschhauser et al., 2014), we calculate the crustal magnetic field at an altitude of 1176 km. The triangle marks the location at which enhanced whistler waves were observed, with a longitude range from −115° to −113° and a latitude range from −52° to −54°. As shown in Figures 2c–e, the crustal magnetic field strength is about 2 nT. Considering that the total observed magnetic field is ~7 nT, this event is clearly influenced by both the crustal magnetic field and the interplanetary magnetic field.

In the quasi-linear theory of wave–particle interaction, wave growth is basically related to pitch angle scattering to smaller pitch angles and a net loss of electron energy (Gendrin, 1981). Meanwhile, wave decay is associated with the pitch angle scattering to larger pitch angles and electron acceleration (Thorne and Horne, 1996; Xiao FL et al., 2007). Hence, in the case of interest, the pitch angle scattering loss is related to the wave growth. Furthermore, Xu SS and Liemohn (2016) have found that local electron loss caused by ionization collisions occurs mainly below an altitude of 150 km. In this event, we thus conclude that the scattering loss of electrons is attributable primarily to whistler waves. This will be discussed in greater detail in the following paragraphs.

3. Methods

Considering that the sampling rate of the MAG is 32 vector samples per second, it is unlikely to obtain the magnetic field component of the wave with frequency higher than 16 Hz. In order to estimate the impacts of whistler mode waves on the electrons, we calculate the electric field expression of local diffusion coefficients by following the previous study Zhang S et al. (2020). It is widely recognized that electrons experience changes in both

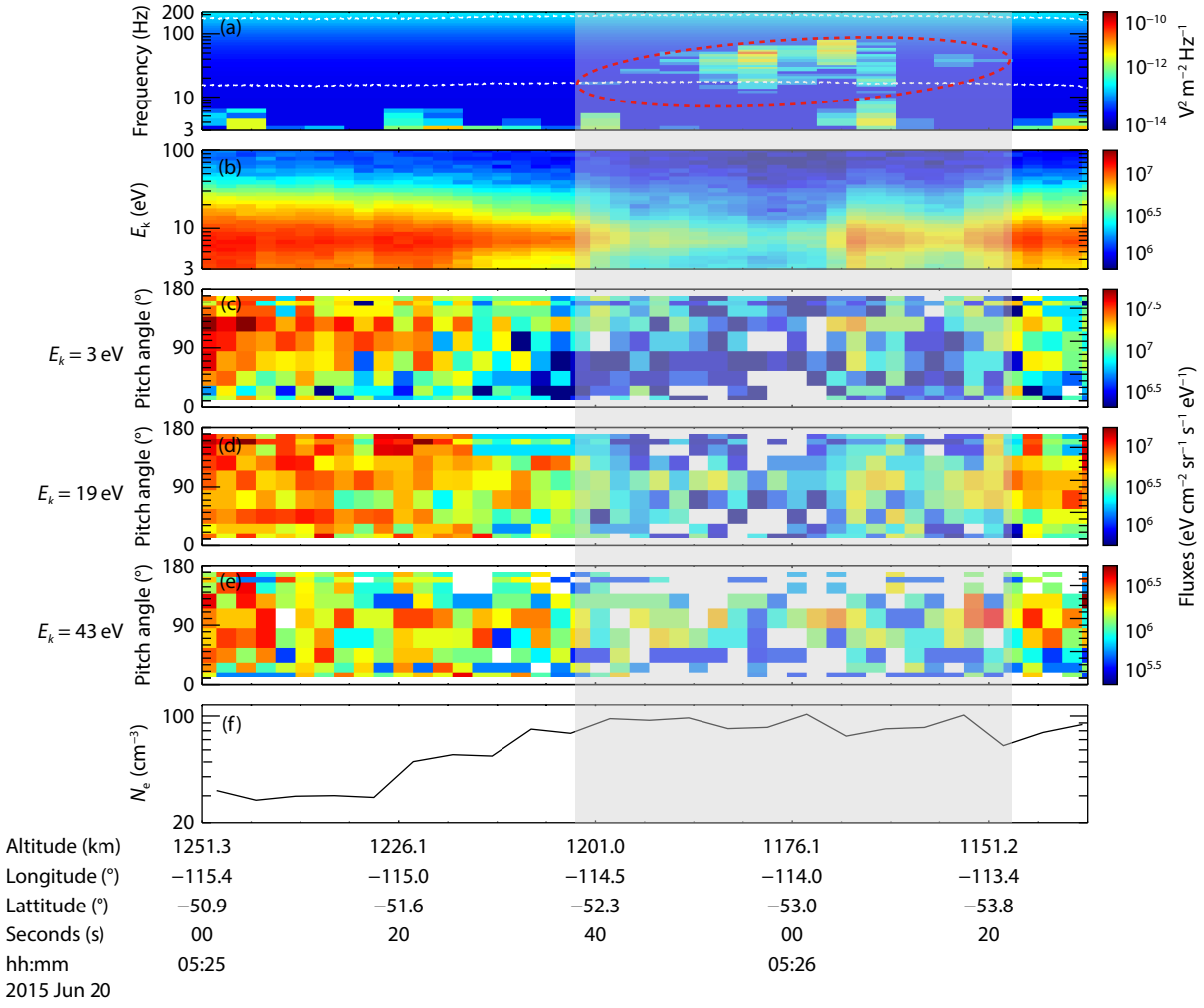

Figure 1. Overview of simultaneous occurrences of the enhanced whistler mode waves and distinct dropout of suprathermal electron fluxes during 05:25:00–05:26:30 UT on June 20, 2015. (a) The electric field spectra of whistler mode waves measured by the LPW instrument. (b) The differential flux of electrons in units of eV/cm^2/s/sr/eV, (c–e) The pitch angle distribution of energetic electrons (3–43 eV) measured by the SWEA instrument. (f) The electron density of whistler mode waves. The upper and lower white dashed lines in Figure 1a indicate the f_{ce} and f_{LH}, respectively. The red dashed line denotes the enhanced whistler mode waves during 05:25:38–05:26:22 UT on June 20, 2015.

energy and pitch angle during wave–electron resonances. When the resonant process is primarily influenced by pitch angle diffusion, it might result in the scattering of electrons towards smaller pitch angles or their eventual loss to the atmosphere. When the energy diffusion process is more pronounced, it enables the acceleration of electrons to higher energy levels. Here, the pitch angle diffusion coefficient is expressed by:

$$D_{aa}^{nX} = \sum_{\omega} \frac{k_{\|}^2 e^2 E^2(\omega)\, g(X)}{4\pi N(\omega)\, \mu^2} \left[\frac{\sin^2\alpha + n\,|\Omega_e|/\gamma\omega}{\cos\alpha}\right]^2 \left[\frac{|\Phi_{n,k}|^2}{|v_{\|} - \partial\omega/\partial k_{\|}|}\right]_X, \quad (1)$$

where $k_{\|}$ represents the parallel wave number, $v_{\|} = v\cos\alpha$, v and α are the velocity and the pitch angle, respectively, $|\Omega_e| = 2\pi f_{ce}$, γ represents the Lorentz factor, μ, e, and n are the refractive index of plasma waves, electron charge, and cyclotron harmonic number, respectively, $E^2(\omega)$ is the wave electric field power spectrum, ω is the wave frequency, $g(X)$ is the wave normal angle distribution, where the wave normal angle is represented by $X = \tan\theta$, where θ is the angle between the background magnetic field and the wave vector, $N(\omega)$ is a normalization factor (Xiao FL et al., 2010), and $|\Phi_{n,k}|^2$ has been derived by Zhang S et al. (2020).

The cross (D_{ap}^{nX}) and momentum (D_{pp}^{nX}) diffusion coefficients using the standard expressions, are as follow:

$$D_{ap}^{nX} = -D_{aa}^{nX}\left[\frac{\sin\alpha\cos\alpha}{\sin^2\alpha + n\,|\Omega_e|/\gamma\omega}\right], \quad (2)$$

$$D_{pp}^{nX} = D_{aa}^{nX}\left[\frac{\sin\alpha\cos\alpha}{\sin^2\alpha + n\,|\Omega_e|/\gamma\omega}\right]^2, \quad (3)$$

the local diffusion coefficients for pitch angle D_{aa}, momentum D_{pp} and crossover D_{ap} can be obtained by integrating over all X and summing over all n, where X is taken from the lower angle (X_l) to the upper angle (X_u). During the resonance process, D_{aa} and D_{pp} are related to the electron scattering and acceleration (Xiao FL et al., 2010), respectively. Specifically, the timescales of the scattering loss (τ_s) and acceleration (τ_a) are generally inversely proportional to the pitch angle and the momentum diffusion coefficient, respectively.

We can obtain the wave electric field power spectrum $E^2(f)$ by

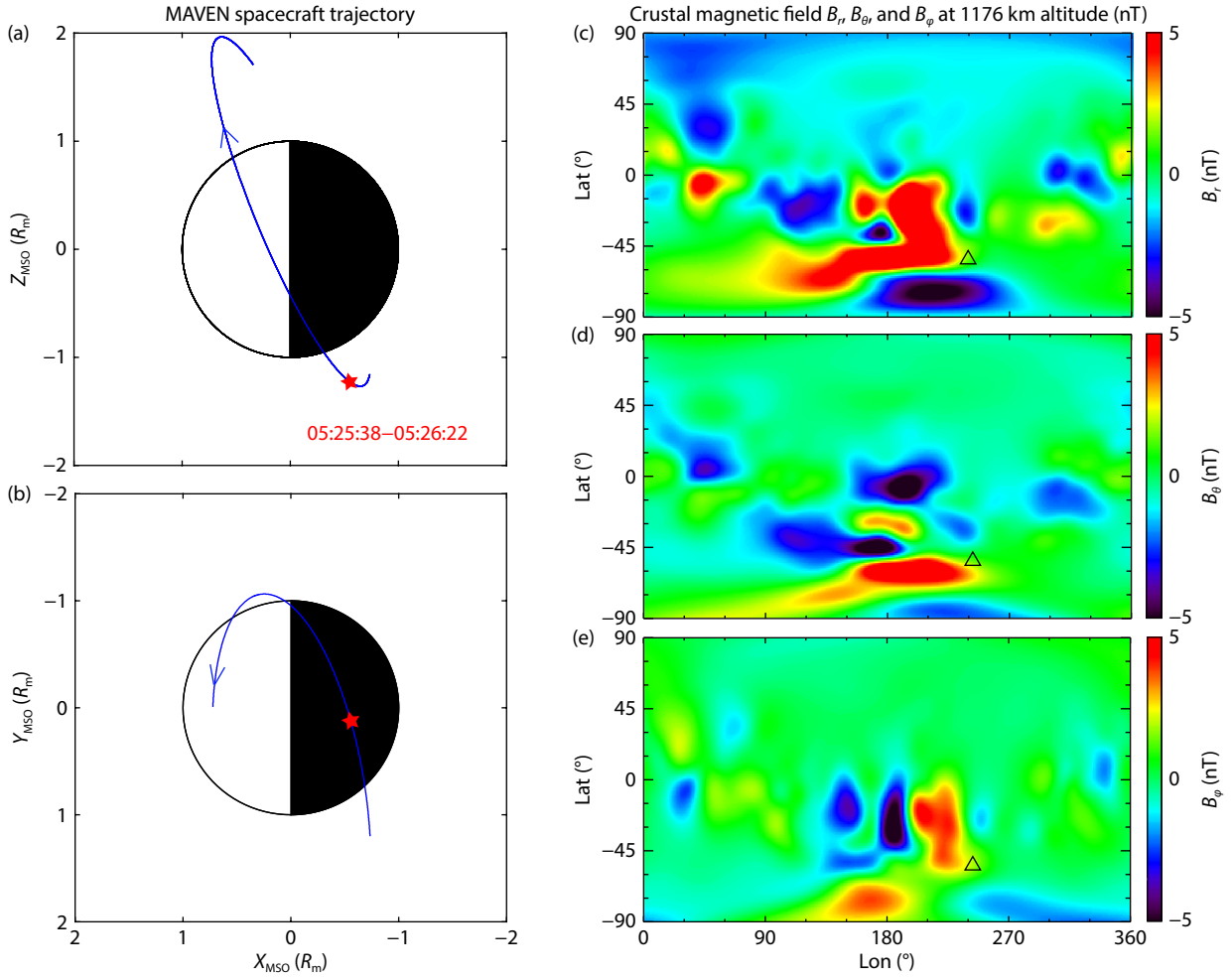

Figure 2. The location of MAVEN orbit (red curve) in the (a) X_{MSO}–Y_{MSO} and (b) X_{MSO}-Z_{MSO} planes in MSO coordinates. The radius of Mars (R_m) is set to be 3393.5 km. The crustal magnetic field components, B_r, B_θ, and B_φ, at an altitude of 1176 km, are shown in (c)–(e), respectively. The triangle marks the position of the spacecraft. The spherical coordinate system used here is identical to the International Astronomical Unions standard for Mars. The r, θ, φ are the radial distance, colatitude, and longitude, respectively.

fitting the observed data to a Gaussian distribution (Lyons et al., 1972), where the wave amplitude E_W is given with frequency, f_m is the peak wave frequency, δf is the half - width, and the band between $f_1 = f_m - \delta f$ and $f_2 = f_m + \delta f$, that is:

$$E^2 = \begin{cases} A^2 \exp[-(f-f_m)^2/(\delta f)^2], & f_1 \leqslant f \leqslant f_2; \\ 0, & \text{otherwise.} \end{cases} \quad (4)$$

$$A^2 = \frac{2E_w^2}{\pi^{1/2}\delta f}\left[\text{erf}\left(\frac{f_2 - f_m}{\delta f}\right) + \text{erf}\left(\frac{f_m - f_1}{\delta f}\right)\right]^{-1}, \quad (5)$$

where A^2 is the normalized parameter, and erf is an error function. As shown in Figure 3, the observed wave spectra are fitted to the Gaussian function by using a least squares method. The observed wave spectra (blue dots) and the fitting result (red line), together with the corresponding parameters, are given for the selected periods from 05:25:49 to 05:26:05 UT on 20 June 2015. Clearly, the fitting result agrees well with the data; the assumption of a Gaussian wave distribution in frequency is justified.

As is well-known, whistler mode waves usually grow fastest along the background magnetic field (Liu S et al., 2015). Analogous to the frequently used treatment (Xiao FL et al., 2014; He JB et al.,

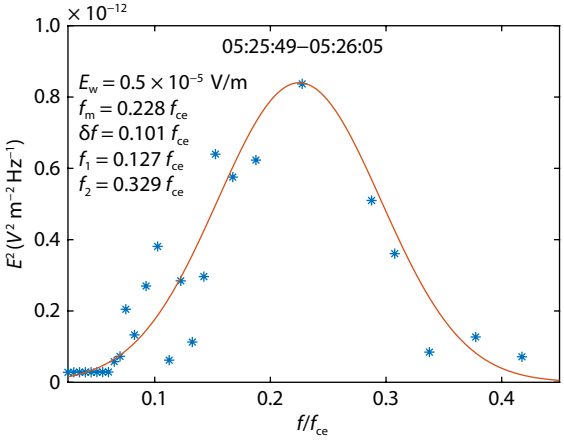

Figure 3. The results of Gaussian fitting. The variation of wave electric field intensity with various frequencies is shown here. The red line is the Gaussian fit curve and the blue dots are the observed wave electric field spectral intensity for the selected periods (05:25:49–05:26:05 UT on 20 June 2015), together with the corresponding fitting wave parameters (the wave amplitude E_W, the peak wave frequency f_m, the half-width δf, and the band between f_1 and f_2).

2021), we also assume that whistler mode waves propagate quasi-parallelly, and we choose the following values of X: $X_l = 0$, $X_u = 1$, the half-width $\delta X = 0.577$, and the peak angle $X_m = 0$. In the present simulation, n is the cyclotron harmonic number, and its value ranges from −5 to 5, where $n = 0$ is the Landau resonance. The averaged ambient magnetic field $B_0 = 7$ nT and $N_e = 86$ cm^{-3} are used in the calculation.

4. Results and Discussion

We show the diffusion coefficients of pitch angle $D_{\alpha\alpha}/p^2$ (Figure 4a), momentum D_{pp}/p^2 (Figure 4b) and cross $|D_{\alpha p}|/p^2$ (Figure 4c) as functions of electron energy E_k and pitch angle α. The maximum value of $D_{\alpha\alpha}/p^2$ can be greater than 10^{-2} s^{-1} over the energy range 3–45 eV; it decreases with increasing E_k.

D_{pp}/p^2 and $|D_{\alpha p}|/p^2$ exhibit similar configurations in the E_k-α frame, with values lower than $D_{\alpha\alpha}/p^2$ by ~100 times and ~10 times, respectively, indicating that pitch angle diffusion dominates over energy transform and momentum diffusion. Efficient pitch angle scattering ($D_{\alpha\alpha}/p^2 > 10^{-4}$ s^{-1}) occurs at lower α for lower E_k and moves to higher α for higher E_k.

Figures 5a–5c illustrate the diffusion coefficients of the three selected energy channels. For lower energies (3 eV), significant pitch angle diffusion ($D_{\alpha\alpha}/p^2 > 10^{-2}$ s^{-1}) is observed primarily in the range $\alpha < 45°$, as shown in Figure 5a. For higher energies (19 eV and 43 eV), the maximum $D_{\alpha\alpha}/p^2$ is observed at higher α (> 60°); effective pitch angle diffusion ($D_{\alpha\alpha}/p^2 > 10^{-4}$ s^{-1}) can still occur in the relatively smaller pitch angles. Based on the first adiabatic invariant, electrons with high pitch angles are usually trapped in the minimum magnetic field. For the closed field, the electrons usually move along the field line and are bounced back between two mirror points. The characteristic bounce period is determined by the magnetic field strength, the pitch angle, and the energy of the electrons, as well as by the length of each specific field line (or specific location). However, data relevant to these details are currently unavailable in the case of interest. More detailed analysis must thus be left to a future study.

For the open interplanetary magnetic field, electrons may escape along the open field line but the timescale is quite long. The wave-particle interaction can reduce the pitch angles of electrons, scattering them to precipitate into the Martian ionosphere and/or facilitating their escape. Because the timescales for escape are potentially much larger than for scattering loss, we suggest that whistler-induced precipitation loss of electrons is the more important phenomenon in cases of interest.

As shown in the line plots of the pitch angle distribution (Figure 6), the flux drops occur dramatically at lower α for 3 eV and move to higher α for 19 eV and 43 eV. Although the simulations are only qualitatively comparable with the observations, they suggest that calculation of diffusion coefficients can explain the decreases in electron flux.

The quantitative study would require solving the Fokker–Planck equations, but current lack of access to realistic initial and boundary conditions makes such solutions highly problematic at this time. We would like to leave that analysis to the future. The calcu-

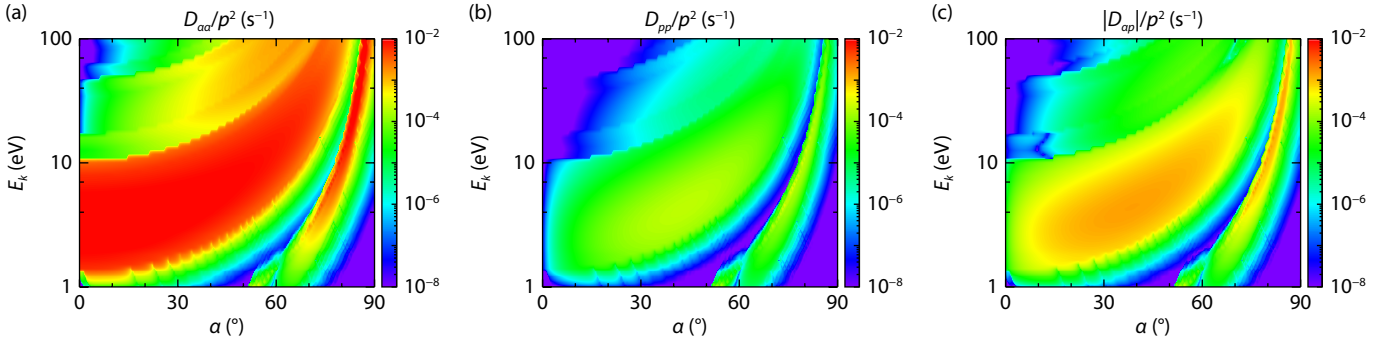

Figure 4. (a–c) The pitch angle diffusion coefficient, the momentum diffusion coefficient, and the cross diffusion coefficient in units of s^{-1}, as a function of energy and pitch angle, respectively. The set parameters correspond to Figure 3.

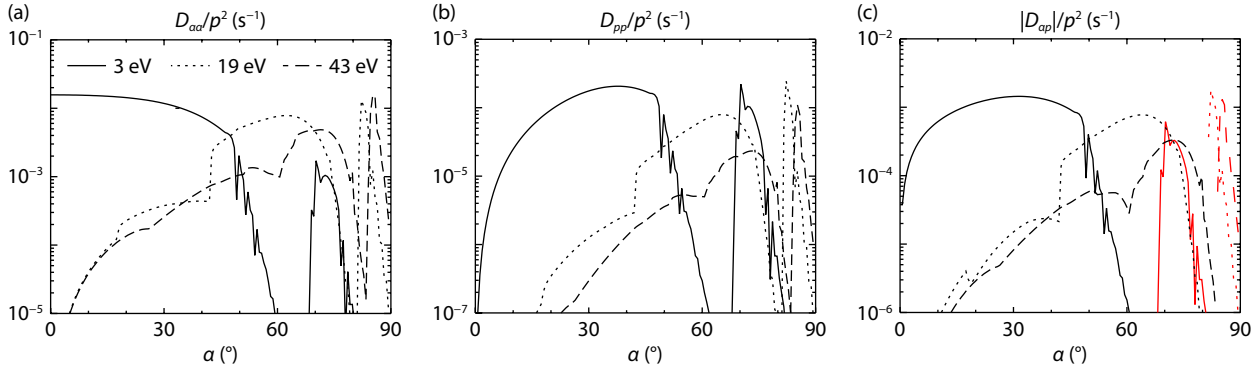

Figure 5. The diffusion coefficients of pitch angle (a), momentum (b), and cross (c) for different electron energy — 3 eV (black solid), 19 eV (dotted line), and 43 eV (dashed line), respectively. The red lines represent the negative value of D_{ap}.

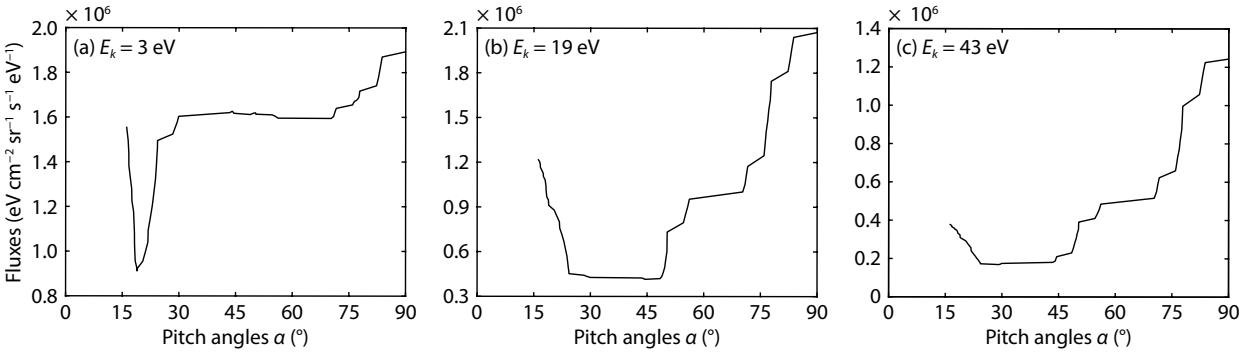

Figure 6. The pitch angle distribution of the selected energy channels (a) 3 eV, (b) 19 eV, and (c) 43 eV at 05:25:49–05:26:05 UT on 20 June 2015, respectively.

lation results presented here, however, are sufficient to suggest that whistler mode waves can scatter suprathermal electrons, which can result in significant scattering losses.

Since the wave normal angle cannot be accurately determined in the absence of detailed magnetic field observations, we analyze the effect of peak wave normal angle X_m variation on diffusion coefficients, as shown in Figure 7. Obviously, all diffusion coefficients remain almost the same for different wave peak angles. As analyzed in detail in the previous studies (Xiao FL et al., 2014; Ding YH et al., 2013), diffusion coefficients depend largely on X_m instead of θ. Therefore, for the events studied in this paper, the results should not significantly change for various wave peak angles because X_m varies very little, indicating that our assumption that the waves are quasi-parallel is reasonable.

5. Conclusions

In this study, simultaneous occurrences of enhanced whistler mode waves and distinct dropouts of suprathermal electron fluxes, in data collected by MAVEN, are reported for the first time. Whistler mode waves with peak spectral density of ~10^{-11} V^2/m^2/Hz were observed by MAVEN between 05:25:38 and 05:26:22 UT on June 20, 2015; at the same time, a significant decrease of suprathermal (3–45 eV) electron fluxes, by one order of magnitude, was observed, exactly corresponding to the intensified whistler mode waves. Based on the observed waves and elec-

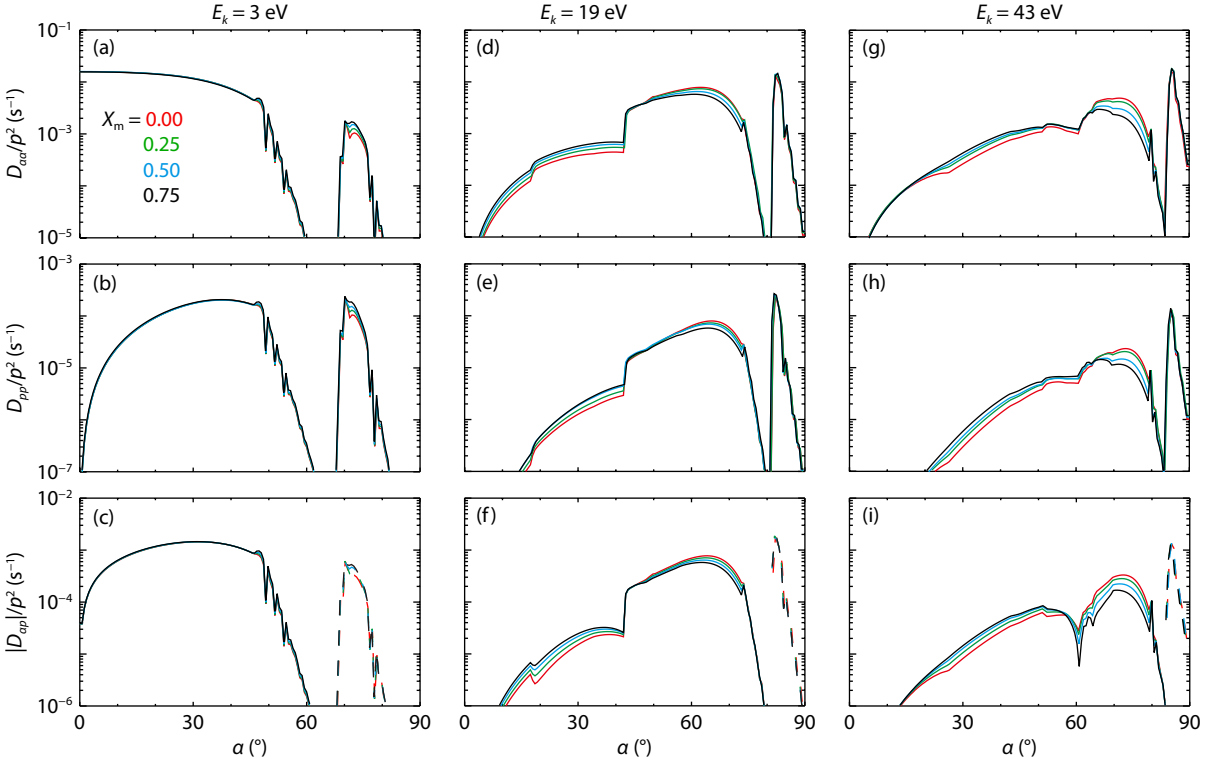

Figure 7. The calculation results of the influence of different peak angles on diffusion coefficients. The red lines, green lines, blue lines, and black lines denote to X_m = 0, 0.25, 0.5, and 0.75, respectively. The dash lines represent the negative value of D_{ap}. The left, middle and right columns represent the calculated diffusion coefficients of different electron energies — 3 eV, 19 eV, and 43 eV, respectively. The other wave parameters are the same as those in Figure 3.

tron data from the MAVEN satellite, we calculated the local diffusion coefficients to study the influence of the whistler mode waves on the suprathermal electrons. Our primary findings are as follows:

(1) The whistler mode waves of frequency ~0.1 f_{ce}–0.5 f_{ce}, occurred exactly corresponding to the pronounced decrease of suprathermal electron fluxes. During the duration of enhanced whistler mode waves, electron fluxes over all measured energies decreased in excess of a factor of ten, especially at small pitch angles. The observational results show that the losses of suprathermal electrons were strongly correlated to the occurrence of the whistler mode waves.

(2) In order to evaluate the impact of the whistler mode waves on the suprathermal electrons, under the assumption that the waves propagate in a quasi-parallel fashion, we calculated the local diffusion coefficients by aid of electric field spectra (due to the lack of magnetic field measurements). The pitch angle diffusion coefficient $D_{\alpha\alpha}/p^2$ can approach 10^{-2} s^{-1}, higher than the momentum diffusion coefficient D_{pp}/p^2 by ~100 times, suggesting that the whistler mode waves generated efficient scattering losses of suprathermal electrons. Simulations also show that the wave normal angle affects the diffusion coefficients insignificantly.

The current study provides direct evidence that Martian whistler mode waves can yield losses of suprathermal electrons, enriching our understanding of the whistler-driven electron dynamics in the Martian magnetosphere.

Acknowledgments

We thank the National Natural Science Foundation of China grants 42230209, 42241136, 42374199, 42204171, 42274212, the Natural Science Foundation of Hunan province Grant 2021JJ20010, 2023JJ20038. We thank all members of the MAVEN mission for their supports. All MAVEN data used in this study are available on the NASA Planetary Data System (https://pds-ppi.igpp.ucla.edu/search/?sc=MAVEN\&facet=SPACECRAFT_NAME).

References

Akalin, F., Gurnett, D. A., Averkamp, T. F., Persoon, A. M., Santolik, O., Kurth, W. S., and Hospodarsky, G. B. (2006). First whistler observed in the magnetosphere of Saturn. *Geophys. Res. Lett.*, *33*(20), L20107. https://doi.org/10.1029/2006GL027019

Andersson, L., Ergun, R. E., Delory, G. T., Eriksson, A., Westfall, J., Reed, H., McCauly, J., Summer, D., and Meyers, D. (2015). The langmuir probe and waves (LPW) instrument for MAVEN. *Space Sci. Rev.*, *195*(1-4), 173–198. https://doi.org/10.1007/s11214-015-0194-3

Connerney, J. E. P., Espley, J., Lawton, P., Murphy, S., Odom, J., Oliversen, R., and Sheppard, D. (2015). The MAVEN magnetic field investigation. *Space Sci. Rev.*, *195*(1-4), 257–291. https://doi.org/10.1007/s11214-015-0169-4

Ding, Y. H., He, Z. G., Zhang, Z. L., and Xiao, F. L. (2013). Influence of wave normal angle on gyroresonance between chorus waves and outer radiation belt electrons. *Sci. China Technol. Sci.*, *56*(11), 2681–2689. https://doi.org/10.1007/s11431-013-5363-6

Fairfield, D. H. (1974). Whistler waves observed upstream from collisionless shocks. *J. Geophys. Res.: Space Physics*, *79*(10), 1368–1378. https://doi.org/10.1029/JA079i010p01368

Fowler, C. M., Agapitov, O. V., Xu, S., Mitchell, D. L., Andersson, L., Artemyev, A., Espley, J., Ergun, R. E., and Mazelle, C. (2020). Localized heating of the Martian topside ionosphere through the combined effects of magnetic pumping by large-scale magnetosonic waves and pitch angle diffusion by whistler waves. *Geophys. Res. Lett.*, *47*(5), e2019GL086408. https://doi.org/10.1029/2019GL086408

Gao, Z. L., Su, Z. P., Zhu, H., Xiao, F. L., Zheng, H. N., Wang, Y. M., Shen, C., and Wang, S. (2016). Intense low-frequency chorus waves observed by Van Allen Probes: fine structures and potential effect on radiation belt electrons. *Geophys. Res. Lett.*, *43*(3), 967–977. https://doi.org/10.1002/2016GL067687

Gendrin, R. (1981). General relationships between wave amplification and particle diffusion in a magnetoplasma. *Rev. Geophys.*, *19*(1), 171–184. https://doi.org/10.1029/RG019i001p00171

Harada, Y., Andersson, L., Fowler, C. M., Mitchell, D. L., Halekas, J. S., Mazelle, C., Espley, J., DiBraccio, G. A., McFadden, J. P., … Jakosky, B. M. (2016). MAVEN observations of electron-induced whistler mode waves in the Martian magnetosphere. *J. Geophys. Res.: Space Physics*, *121*(10), 9717–9731. https://doi.org/10.1002/2016JA023194

He, J. B., Jin, Y. Y., Xiao, F. L., He, Z. G., Yang, C., Xie, Y. Q., He, Q., Wang, C. Z., Shang, X. J., … Zhang, S. (2021). The influence of various frequency chorus waves on electron dynamics in radiation belts. *Sci. China Technol. Sci.*, *64*(4), 890–897. https://doi.org/10.1007/s11431-020-1750-6

He, Q., Liu, S., Xiao, F. L., Gao, Z. L., Li, T., Shang, X. J., Zhou, Q. H., Yang, C., and He, Y. H. (2022). Observations and parametric study on the role of plasma density on extremely low-frequency chorus wave generation. *Sci. China Technol. Sci.*, *65*(11), 2649–2657. https://doi.org/10.1007/s11431-021-2030-7

Hospodarsky, G. B., Averkamp, T. F., Kurth, W. S., Gurnett, D. A., Menietti, J. D., Santolik, O., and Dougherty, M. K. (2008). Observations of chorus at Saturn using the Cassini Radio and Plasma Wave Science instrument. *J. Geophys. Res.: Space Physics*, *113*(A12), A12206. https://doi.org/10.1029/2008JA013237

Jakosky, B. M., Lin, R. P., Grebowsky, J. M., Luhmann, J. G., Mitchell, D. F., Beutelschies, G., Priser, T., Acuna, M., Andersson, D., … Zurek. R. (2015a). The Mars Atmosphere and Volatile Evolution (MAVEN) Mission. *Space Sci. Rev.*, *195*, 3–48. https://doi.org/10.1007/s11214-015-0139-x

Jakosky, B. M., Grebowsky, J. M., Luhmann, J. G., Connerney, J., Eparvier, F., Ergun, R., Halekas, J., Larson, D., Mahaffy, J., … Yelle, R. (2015b). MAVEN observations of the response of Mars to an interplanetary coronal mass ejection. *Science*, *350*(6261), aad0210. https://doi.org/10.1126/science.aad0210

Jin, T. F., Ni, B. B., Kong, L. G., Zhang, A. B., Li, L., Fu, S., Cao, X., Li, W. Y., Tang, B. B., … Ma, J. J. (2023). Proton pitch angle distributions in the Martian induced magnetosphere: A survey of Tianwen-1 Mars Ion and Neutral Particle Analyzer observations. *Earth Planet. Phys.*, *7*(5), 533–539. https://doi.org/10.26464/epp2023072

Kumari, J., and Pandey, R. S. (2018). Whistler mode waves for ring distribution with A. C. electric field in inner magnetosphere of Saturn Astrophys. *Space Sci.*, *363*(12), 249. https://doi.org/10.1007/s10509-018-3466-z

Li, W., Thorne, R. M., Angelopoulos, V., Bonnell, J. W., McFadden, J. P., Carlson, C. W., LeContel, O., Roux, A., Glassmeier, K. H., and Auster, H. U. (2009). Evaluation of whistler-mode chorus intensification on the nightside during an injection event observed on the THEMIS spacecraft. *J. Geophys. Res.: Space Physics*, *114*(A1), A00C14. https://doi.org/10.1029/2008JA013554

Li, W., Thorne, R. M., Bortnik, J., Reeves, G. D., Kletzing, C. A., Kurth, W. S., Hospodarsky, G. B., Spence, H. E., Blake, J. B., … Thaller, S. A. (2013). An unusual enhancement of low-frequency plasmaspheric hiss in the outer plasmasphere associated with substorm-injected electrons. *Geophys. Res. Lett.*, *40*(15), 3798–3803. https://doi.org/10.1002/grl.50787

Li, W., Ma, Q., Shen, X. C., Zhang, X. J., Mauk, B. H., Clark, G., Allegrini, F., Kurth, W. S., Hospodarsky, G. B., … Bolton, S. J. (2021). Quantification of diffuse auroral electron precipitation driven by whistler mode waves at Jupiter. *Geophys. Res. Lett.*, *48*(19), e2021GL095457. https://doi.org/10.1029/2021GL095457

Liu, S., Xiao, F. L., Yang, C., He, Y. H., Zhou, Q. H., Kletzing, C. A., Kurth, W. S., Hospodarsky, G. B., Spence, H. E., … Wygant, J. R. (2015). Van Allen Probes observations linking radiation belt electrons to chorus waves during 2014 multiple storms. *J. Geophys. Res.: Space Physics*, *120*(2), 938–948. https://doi.org/10.1002/2014JA020781

Liu, S., Xie, Y. Q., Zhang, S., Shang, X. J., Yang, C., Zhou, Q. H., He, Y. H., and Xiao, F. L. (2020). Unusual loss of Van Allen belt relativistic electrons by extremely low-frequency chorus. *Geophys. Res. Lett.*, *47*(18), e2020GL089994. https://doi.org/10.1029/2020GL089994

Lyons, L. R., Thorne, R. M., and Kennel, C. F. (1972). Pitch-angle diffusion of radiation belt electrons within the plasmasphere. *J. Geophys. Res.: Space Physics*, *77*(19), 3455–3474. https://doi.org/10.1029/JA077i019p03455

Mitchell, D. L., Mazelle, C., Sauvaud, J. A., Thocaven, J. J., Rouzaud, J., Fedorov, A., Rouger, P., Toublanc, D., Taylor, E., … Jakosky, B. M. (2016). The MAVEN solar wind electron analyzer. *Space Sci. Rev.*, *200*(1-4), 495–528. https://doi.org/10.1007/s11214-015-0232-1

Morschhauser, A., Lesur, V., and Grott, M. (2014). A spherical harmonic model of the lithospheric magnetic field of Mars. *J. Geophys. Res.: Planets.*, *119*(6), 1162–1188. https://doi.org/10.1002/2013JE004555

Nagy, A. F., Winterhalter, D., Sauer, K., Cravens, T. E., Brecht, S., Mazelle, C., Crider, D., Kallio, E., Zakharov, A., … Trotignon, J. G. (2004). The plasma environment of mars. *Space Sci. Rev.*, *111*(1-2), 33–114. https://doi.org/10.1023/B:SPAC.0000032718.47512.92

Ni, B. B., Huang, J., Ge, Y. S., Cui, J., Wei, Y., Gu, X. G., Fu, S., Xiang, Z., Zhao, Z. Y. (2018). Radiation belt electron scattering by whistler-mode chorus in the Jovian magnetosphere: Importance of ambient and wave parameters. *Earth Planet. Phys.*, *2*(1), 1–14. https://doi.org/10.26464/epp2018001

Scarf, F. L., Gurnett, D. A., and Kurth, W. S. (1979). Jupiter plasma wave observations: an initial voyager 1 overview. *Science*, *204*(4396), 991–995. https://doi.org/10.1126/science.204.4396.991

Shane, A., Liemohn, M., Florie, C., and Xu, S. S. (2019). Misbehaving high-energy electrons: evidence in support of ubiquitous wave-particle interactions on dayside Martian closed crustal magnetic fields. *Geophys. Res. Lett.*, *46*(21), 11689–11697. https://doi.org/10.1029/2019GL084919

Shane, A., and Liemohn, M. (2021). Whistler wave Interactions with superthermal electrons on martian crustal magnetic fields: bounce-averaged diffusion coefficients and time scales. *J. Geophys. Res.: Space Physics*, *126*(6), e2021JA029118. https://doi.org/10.1029/2021JA029118

Shane, A. D., and Liemohn, M. W. (2022). Modeling wave-particle interactions with photoelectrons on the dayside crustal fields of mars. *Geophys. Res. Lett.*, *49*(2), e2021GL096941. https://doi.org/10.1029/2021GL096941

Shang, X. J., Liu, S., Chen, L. J., Gao, Z. L., Wang, G., He, Q., Li, T., and Xiao, F. L. (2021). ULF-modulation of whistler-mode waves in the inner magnetosphere during solar wind compression. *J. Geophys. Res.: Space Physics*, *126*(8), e2021JA029353. https://doi.org/10.1029/2021JA029353

Shprits, Y. Y., Menietti, J. D., Gu, X., Kim, K. C., and Horne, R. B. (2012). Gyroresonant interactions between the radiation belt electrons and whistler mode chorus waves in the radiation environments of Earth, Jupiter, and Saturn: a comparative study. *J. Geophys. Res.: Space Physics*, *117*(A11), A11216. https://doi.org/10.1029/2012JA018031

Shprits, Y. Y., Menietti, J. D., Drozdov, A. Y., Horne, R. B., Woodfield, E. E., Groene, J. B., de Soria-Santacruz, M., Averkamp, T. F, Garrett, H., … and Gurnett, D. A. (2018). Strong whistler mode waves observed in the vicinity of Jupiter's moons. *Nat. Commun.*, *9*(1), 3131. https://doi.org/10.1038/s41467-018-05431-x

Stix, T. H. (1992). *Waves in Plasmas*. New York: American Institute of Physics Melville.

Thorne, R. M., and Horne, R. B. (1996). Whistler absorption and electron heating near the plasmapause. *J. Geophys. Res.: Space Physics*, *101*(A1), 4917–4928. https://doi.org/10.1029/95JA03671

Wan, W. X., Wang, C., Li, C. L., Wei, Y. and Liu, J. J. (2020). The payloads of planetary physics research onboard China's First Mars Mission (Tianwen-1). *Earth Planet. Phys.*, *4*(4), 331–332. https://doi.org/10.26464/epp2020052

Wei, X. H., Cao, J. B., Zhou, G. C., Santolík, O., Rème, H., Dandouras, I., Cornilleau-Wehrlin, N., Lucek, E., Carr, C. M., and Fazakerley, A. (2007). Cluster observations of waves in the whistler frequency range associated with magnetic reconnection in the Earth's magnetotail. *J. Geophys. Res.: Space Physics*, *112*(A10), A10225. https://doi.org/10.1029/2006JA011771

Xiao, F. L., Chen, L. J., Zheng, H. N., and Wang, S. (2007). A parametric ray tracing study of superluminous auroral kilometric radiation wave modes. *J. Geophys. Res.: Space Physics*, *112*(A10), A10214. https://doi.org/10.1029/2006JA012178

Xiao, F. L., Li, J. Q., Tang, L. J., He, Y. H., and Li, J. F. (2009a). Effect of chorus latitudinal distribution on evolution of outer radiation belt electrons. *Plasma Sci. Technol.*, *11*(5), 544–549. https://doi.org/10.1088/1009-0630/11/5/06

Xiao, F. L., Su, Z. P., Zheng, H. N., and Wang, S. (2009b). Modeling of outer radiation belt electrons by multidimensional diffusion process. *J. Geophys. Res.: Space Physics*, *114*(A3), A03201. https://doi.org/10.1029/2008JA013580

Xiao, F. L., Su, Z. P., Chen, L. X., Zheng, H. N., and Wang, S. (2010). A parametric study on outer radiation belt electron evolution by superluminous R-X mode waves. *J. Geophys. Res.: Space Physics*, *115*(A10), A10217. https://doi.org/10.1029/2010JA015374

Xiao, F. L., Yang, C., He, Z. G., Su, Z. P., Zhou, Q. H., He, Y. H., Kletzing, C. A., Kurth, W. S., Hospodarsky, G. B., … and Wygant, J. R. (2014). Chorus acceleration of radiation belt relativistic electrons during March 2013 geomagnetic storm. *J. Geophys. Res.: Space Physics*, *119*(5), 3325–3332. https://doi.org/10.1002/2014JA019822

Xu, S. S., and Liemohn, M. W. (2015). Superthermal electron transport model for Mars. *Earth Space Sci.*, *2*(3), 47–64. https://doi.org/10.1002/2014EA000043

Xu, S. S., Liemohn, M., Bougher, S., and Mitchell, D. (2016). Martian high-altitude photoelectrons independent of solar zenith angle. *J. Geophys. Res.: Space Physics 121*(4), 3767-3780. https://doi.org/10.1002/2015JA022149

Yang, Q. W., Yang, C., He, Y. H., Liu, S., Zhou, Q. H, and Xiao, F. L. (2016). Magnetospheric chorus wave instability induced by relativistic kappa-type distributions. *Sci. China Technol. Sci.*, *59*(11), 1739–1745. https://doi.org/10.1007/s11431-016-0161-2

Zhang, S., Shang, X. J., He, Y. H., Liu, S., and Xiao, F. L. (2020). Dominant roles of high harmonics on interactions between AKR and radiation belt relativistic electrons. *Geophys. Res. Lett.*, *47*(16), e2020GL088421. https://doi.org/10.1029/2020GL088421

Zhao, H., and Li, X. (2013). Modeling energetic electron penetration into the slot region and inner radiation belt. *J. Geophys. Res.: Space Physics*, *118*(11), 6936–6945. https://doi.org/10.1002/2013JA019240

Zhao, Y. W., Xiang, Z., Gu, X. D., Ni, B. B., Ma, X., Lou, Y. Q., Jiao, L. H., Zhou, R. X., Guo, D. Y., Liu, Y. X. Z., and Dong, J. H. (2022). Simultaneous occurrence of four magnetospheric wave modes and the resultant combined scattering effect on radiation belt electrons. *Earth Planet. Phys.*, *6*(6), 563–575. https://doi.org/10.26464/epp2022050